

Chaotic delocalization of two interacting particles in the classical Harper model

D.L. Shepelyansky

Laboratoire de Physique Théorique du CNRS, IRSAMC, Université de Toulouse, CNRS, UPS, 31062 Toulouse, France

Dated: April 12, 2016

Abstract. We study the problem of two interacting particles in the classical Harper model in the regime when one-particle motion is absolutely bounded inside one cell of periodic potential. The interaction between particles breaks integrability of classical motion leading to emergence of Hamiltonian dynamical chaos. At moderate interactions and certain energies above the mobility edge this chaos leads to a chaotic propulsion of two particles with their diffusive spreading over the whole space both in one and two dimensions. At the same time the distance between particles remains bounded by one or two periodic cells demonstrating appearance of new composite quasi-particles called chaons. The effect of chaotic delocalization of chaons is shown to be rather general being present for Coulomb and short range interactions. It is argued that such delocalized chaons can be observed in experiments with cold atoms and ions in optical lattices.

PACS. 05.45.Mt Quantum chaos; semiclassical methods – 72.15.Rn Localization effects (Anderson or weak localization) – 67.85.-d Ultracold gases

1 Introduction

The Harper model describes a quantum dynamics of an electron in a two-dimensional periodic potential (2D) and a perpendicular magnetic field [1]. Due to periodicity of potential the problem can be reduced to the Schrödinger equation on a discrete quasiperiodic one-dimensional (1D) lattice. This equation is characterized by a dimensionless Planck constant \hbar determined by a magnetic flux through the lattice cell. The fractal spectral properties of this system have been discussed in [2] and the fractal structure of its spectrum was directly demonstrated in [3].

For typical irrational flux values the system has a Metal-Insulator Transition (MIT) established by Aubry and André [4]. The MIT takes place when the amplitude λ of the quasiperiodic potential (with hopping being unity) is changed from $\lambda < 2$ (metallic or delocalized phase) to $\lambda > 2$ (insulator or localized phase). A review of the properties of the Aubry-André model can be found in [5] and the mathematical prove of MIT is given in [6]. The stationary Schrödinger equation of the system has the form

$$\lambda \cos(\hbar n + \beta) \phi_n + \phi_{n+1} + \phi_{n-1} = E \phi_n \quad (1)$$

or in the operator representation

$$\hat{H} \psi = [\lambda \cos \hat{x} + 2 \cos \hat{p}] \psi = E \psi, \quad (2)$$

where \hat{p}, \hat{x} are momentum and coordinate operators with the usual commutator $[\hat{p}, \hat{x}] = -i\hbar$ [5].

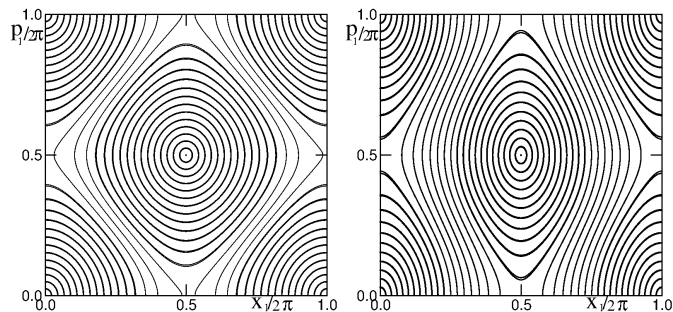


Fig. 1. Phase space of the one-particle classical Harper model at $\lambda = 2.5$ (left panel) and $\lambda = 4.5$ (right panel); curves correspond to 60 trajectories with different initial conditions. Only one cell of the periodic phase space is shown.

From the view point of classical dynamics the critical value $\lambda = 2$ is very natural. Indeed, the dynamics is described by the classical Hamiltonian

$$H(p, x) = \lambda \cos x + 2 \cos p = E, \quad (3)$$

with commuting conjugated variables (p, x) in (2). For $\lambda > 2$ the maximal value of kinetic term $K = 2 \cos p$ is smaller than the potential barrier $V = \lambda \cos x$ and a particle cannot overcome the barrier being localized in coordinate space (all equipotential curves are vertical on the phase plane (p, x)). In the opposite case $\lambda < 2$ the maximal value of potential barrier is smaller than the kinetic term and at certain energies a particle can propagate

ballistically along x . Examples of phase space curves for the classical localized phase at $\lambda > 2$ are shown in Figure 1. The energy of the system is restricted to the interval $-2 - \lambda \leq E \leq 2 + \lambda$. At $\lambda = 2$ and $E = 0$ the separatrix lines $p_1 = x_1 + \pi + 2\pi m_1$, $p_1 = -x_1 + \pi + 2\pi m_2$ go to infinity covering the whole phase space (m_1, m_2 are integers).

Of course, the behavior of quantum system is much more subtle due to presence of quantum tunneling so that highly skillful mathematical methods are required to prove quantum localization of eigenstates at typical irrational flux value $\hbar/2\pi$ and to extend analysis to more general hopping terms (see [6,7,8]). The numerical studies of the quantum model can be found at [9,10].

The investigation of interaction effects between particles in the 1D quantum Harper model was started in [11] with the Hubbard interaction of Two Interacting Particles (TIP). It was found that the interaction creates TIP localized states in the regime when all eigenstates of noninteracting particles are delocalized in the 1D Harper model (metallic phase at $\lambda < 2$). Further studies also found enhancement of localization effects in presence of interactions [12,13]. This localization enhancement is opposite to the TIP effect in disordered systems where the interactions increase the TIP localization length in 1D [14,15,16,17,18,20,23] or even lead to delocalization of TIP pairs for dimensions $d \geq 2$ [19,21,22]. Thus interactions between two particles in systems with disorder can even destroy the Anderson localization existing for noninteracting particles. The tendency in the 1D Harper model seemed to be an opposite one.

Thus the results obtained in [24] on the appearance of delocalized TIP pairs in the 1D quantum Harper model, for certain particular values of interaction strength and energy, in the regime, when all one-particle states are exponentially localized, is really surprising. The recent advanced studies confirmed the existence of so called Freed by Interaction Kinetic States (FIKS) with delocalized quasiballistic FIKS pairs, existing at various irrational flux values, propagating over the whole large system sizes [25]. The studies of TIP on the 2D Harper model showed the presence of subdiffusive delocalization of TIP but found no signs of quasiballistic states [26].

At present the skillful experiments with cold atoms in optical lattices allowed to realize the 1D Harper model, to observe there the MIT transition for noninteracting particles and to perform studies of interactions [27,28,29]. The first steps in experimental study of the 2D Harper model are reported recently [30].

The Harper Hamiltonian (2) appears also in such solid-state systems like incommensurate crystals where a free electron propagation in a finite energy band ($E = 2 \cos p$) is affected by atomic charges creating an effective periodic potential ($V(x) = \lambda \cos x$) [31,32,33]. Indeed, the energy band spectrum like $E \sim \cos p$ naturally appears in semiconductor heterostructures and superlattices (see e.g. [34]). Hence, the investigation of interaction effects in the Harper model can be relevant also for incommensurate crystals.

In view of this theoretical and experimental progress it is important to obtain a better understanding of the physical origins of FIKS pairs and TIP delocalization in the Harper model. With this aim we study the properties of TIP in the classical Harper model considering the Hamiltonian dynamics in the classical conservative systems with two (and four) degrees of freedom in the 1D (and 2D) Harper model. We show that at rather generic conditions the interactions destroy classical integrability of motion and localization, leading to chaos and chaotic propulsion of TIP characterized by a diffusive spreading in coordinate space.

The paper is composed as follows: Section 2 describes TIP with Coulomb interactions in the 1D Harper model, Section 3 describes TIP with a short range interaction in 1D, Section 4 describes TIP with Coulomb interactions in the 2D Harper model and the discussion of the results is presented in Section 5.

2 TIP with Coulomb interactions in 1D

The classical TIP Hamiltonian in the 1D Harper model reads:

$$H(p_1, p_2, x_1, x_2) = 2(\cos p_1 + \cos p_2) + \lambda(\cos x_1 + \cos x_2) + U/((x_2 - x_1)^2 + b^2)^{1/2} . \quad (4)$$

Here U is a strength of Coulomb interaction and b is a certain screening or regularization length appearing due to quantum smoothing or effective finite distance in 2D. In the following we keep $b = 1$ since the results are not very sensitive to b value as soon as b is smaller than the lattice period $d = 2\pi$ in space. Here we use dimensionless units where the lattice spatial period is $d = 2\pi$. In physical units the interaction strength can be measured as $U = 2\pi e^2/d$ where e is electron charge and d the lattice period.

At $U = 0$ we have integrable dynamics of noninteracting particles which is bounded in space x inside one periodic cell at any energy. For finite U values the invariant Kolmogorov-Arnold-Moser (KAM) curves start to be destroyed by interactions with appearing of chaotic motion [35,36] with unbounded diffusion of pairs in x space. It is clear that particles can diffuse only in pairs since individual particles are localized inside one lattice period due to integrability of one-particle dynamics and energy restrictions discussed above. From the energetic viewpoint a kinetic energy of two particles $K = 2(\cos p_1 + \cos p_2)$ can become larger than a potential barrier $V = \lambda(\cos x_1 + \cos x_2)$ in effective 2D space of TIP that can allow to overcome this barrier leading to extended propagation of TIP. We call such delocalized TIP pairs chaons since they are generated by chaos.

We note that in presence of interactions the allowed energy band of the Hamiltonian (4) is $-4 - 2\lambda \leq E \leq 4 + 2\lambda + U$ (due to band energy structure and symmetry $p \rightarrow -p, x \rightarrow -x$ we consider only the repulsive case $U \geq 0$; the attractive case $U < 0$ has the same behavior as at $U > 0$).

The Hamiltonian dynamics of (4) is integrated numerically by the Runge-Kutta method with a typical time step

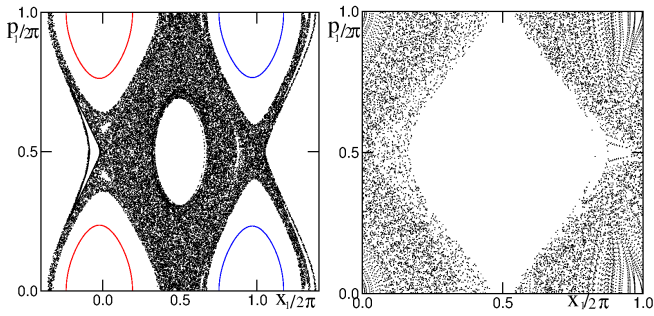


Fig. 2. Poincaré sections for TIP at $\lambda = 2.5$ and $U = 1$; left panel: 3 trajectories are shown at energies $E = -2.4$ (black points), -0.046 (red points), -0.07 (blue points) up to times $t = 2 \times 10^5$; right panel: one trajectory at $E = 0.42$ (black points) up to $t = 10^5$. The vertical axis shows the fractional part of $p_1/2\pi \pmod{1}$ and the horizontal axis shows $x_1/2\pi$ (left panel, no fraction) and the fractional part of $x_1/2\pi \pmod{1}$ (right panel, $x_1/2\pi$ varies in the range $(-12, 1)$); the sections are taken at a fractional part $p_2/2\pi = 1/2$ and $dp_2/dt > 0$; white area in the right panel corresponds to energy forbidden region.

$\Delta t = 0.01$ and the relative accuracy of energy conservation being around 10^{-8} for times $t \sim 100$ and better than 10^{-5} for $t \sim 10^6$.

Examples of Poincaré sections [36] at a moderate interaction $U = 1$ are shown in Figure 2 for $\lambda = 2.5$ when noninteracting particles are localized inside one coordinate cell. At some energies the dynamics remains integrable ($E = -0.046, -0.07$), it can be also chaotic but bounded inside one or two coordinate cells ($E = -2.4$) or to be chaotic and unbounded in coordinate space ($E = 0.42$). The emergence of chaos induced by interactions is rather natural since the one-particle system is strongly nonlinear.

Typical examples of trajectories in coordinate and momentum space are shown in Figure 3 for $\lambda = 2.5$ and 4.5 . On a scale of a few cells there is a complex, chaotic dynamics of TIP inside a given cell leading to chaotic transitions to nearby cells (top row). In this manner a chaotic propulsion of TIP generates TIP propagation along x -axis. In all cases of delocalized TIP at $U \leq 20$ the distance between particles is not exceeding $\Delta x_M = \max |x_2 - x_1| = 2$ (middle row). While in x -direction the propagation is diffusive (see Figures 4, 5 below) the spreading in momentum remains quasiballistic with approximately linear growth of p_1, p_2 with time (bottom row); for momentum this is not very surprising since there is a ballistic growth of p even for one particle (see Figure 1).

The diffusive nature of TIP propagation and spreading along x is directly illustrated in Figures 4, 5. Indeed, the second moment $\sigma = \langle (x_1^2 + x_2^2)/2 \rangle$ grows linearly with time as $\sigma = Dt$, both for $\lambda = 2.5$ and 4.5 (see Figure 4). These data are averaged over 10^3 trajectories.

The probability or density distribution $W(x, t)$ of these trajectories in x is well described by the Fokker-Planck equation

$$\partial W(x, t)/\partial t = (D/2)\partial^2 W(x, t)/\partial x^2. \quad (5)$$

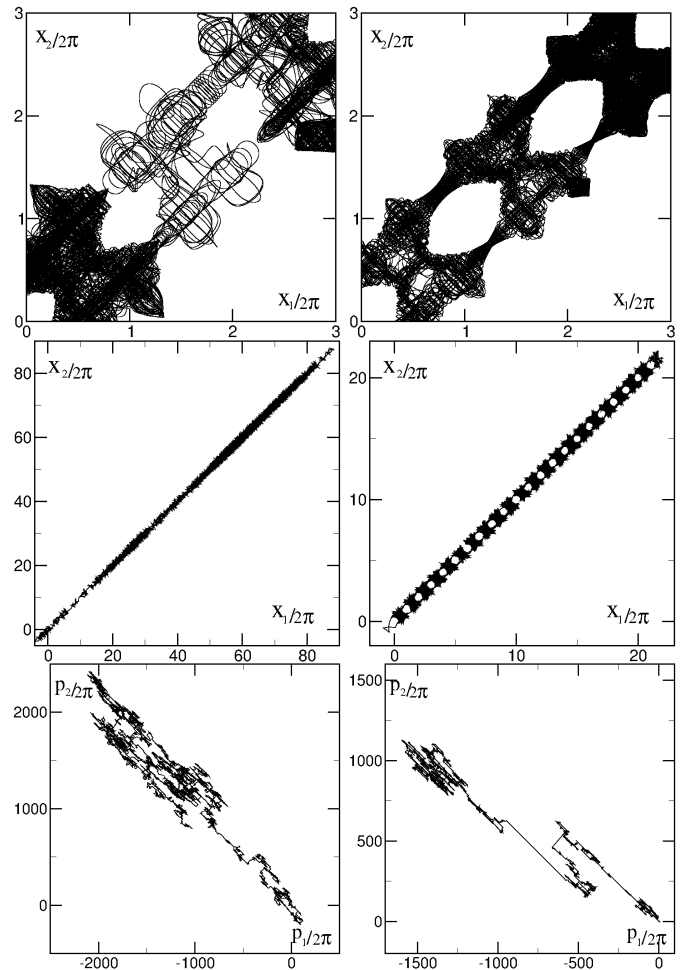


Fig. 3. Dynamics of a typical TIP trajectory in the classical Harper model is shown for $\lambda = 2.5$, $U = 6$, $E = 1.884$ (left column) and $\lambda = 4.5$, $U = 12$, $E = 3.876$ (right column). Top row shows TIP dynamics in plane (x_1, x_2) on small scale; middle row shows the same on large scale up to times $t = 10^6$; bottom row shows TIP dynamics in (p_1, p_2) on large scale up to times $t = 10^6$; positions are shown with a time step 0.01 (top) and 10 (middle, bottom).

Indeed, the analytic solution is in a good agreement with the numerical result obtained by averaging over 10^3 trajectories of (4) at times $t \leq 10^5$ (see Figure 5).

To determine the dependence of measure μ and diffusion coefficient D on TIP energy E we follow $N = 10^4$ trajectories till time $t = 10^6$. Initially at $t = 0$ all trajectories are homogeneously distributed in the phase space with TIP being inside the same cell. Those trajectories with displacements from initial positions being less than the size of 2 cells are considered as non-diffusive. The total measure μ of diffusive trajectories at all energies N_d is determined as a fraction $\mu = N_d/N$. The differential distribution $d\mu/dE$ is obtained from a histogram with energy interval $\Delta E = 0.1$. The obtained dependence $d\mu/dE$ on E is shown in Figure 6 for $\lambda = 2.5; 4.5$ at different interactions. The total measure μ is rather small at weak interactions ($\mu = 0.025$ at $U = 1, \lambda = 2.5$), it increases

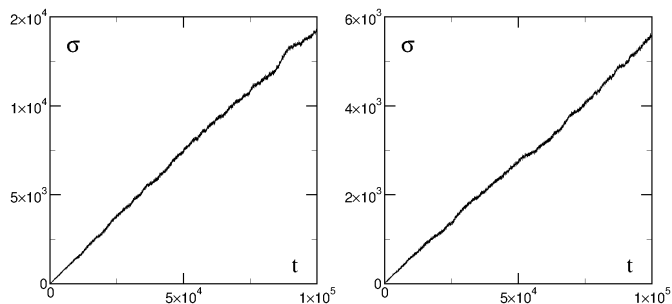


Fig. 4. Time dependence of the second moment $\sigma(t) = \langle ((x_1)^2 + (x_2)^2)/2 \rangle$ averaged over 10^3 orbits taken in a vicinity of trajectories of Fig. 2 at $\lambda = 2.5$, $U = 6$, $E \approx 1.884$ (left panel) and $\lambda = 4.5$, $U = 12$, $E \approx 3.876$ (right panel). The fit gives the diffusion rate $\sigma = Dt + const$ with $D = 0.143 \pm 3.2 \times 10^{-5}$ (left panel) and $0.0543 \pm 1.4 \times 10^{-4}$ (right panel).

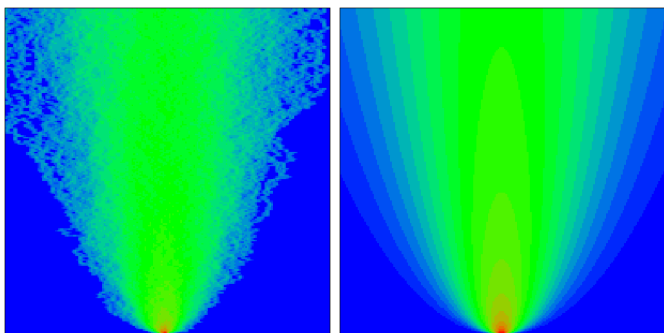


Fig. 5. One-particle density distribution over coordinate range $(-60 \leq x_{1,2}/2\pi \leq 60)$ on horizontal axis and time interval $0 \leq t \leq 10^5$ on vertical axis. Left panel: data are averaged over 10^3 TIP orbits of Fig. 3 at $\lambda = 2.5$, $U = 6$, $E \approx 1.884$; right panel: the theoretical distribution $W(x, t) = \exp(-x^2/2Dt)/\sqrt{2\pi Dt}$ of the diffusion equation (5) with the diffusion rate $D = 0.143$ of Fig. 4 shown in the same range as in left panel; color is proportional to density changing from zero (blue) to maximum (red).

till optimal values of $U \approx 12$ being comparable with the total energy band width $E_B = 8 + 4\lambda = 18$, and then decreases with U . The maximum of $d\mu/dE$ is located approximately at energy $E_{max} \approx U/\pi$ since at $U = 0$ the most deformed KAM curves are located at $E \approx 0$ and on average the distance between particles inside one cell is π giving a corresponding energy shift.

We note that for $\lambda = 2.5$, $U = 6$ the measure of diffusive orbits decreases from $\mu = 0.2295$ down to $\mu = 0.09$ if the initial positions of second particle are taken in nearby cell ($x_2 \rightarrow x_2 + 2\pi$). Indeed, on average this gives a reduction of interactions decreasing the measure of chaos. We should note that at these parameters for all diffusive trajectories the maximal separation of particles during time evolution is not exceeding the size of two cells ($|x_2 - x_1|/2\pi < 2$).

The energy dependence of diffusion coefficient $D(E)$ is shown in Figure 7. The maxima of D are approximately

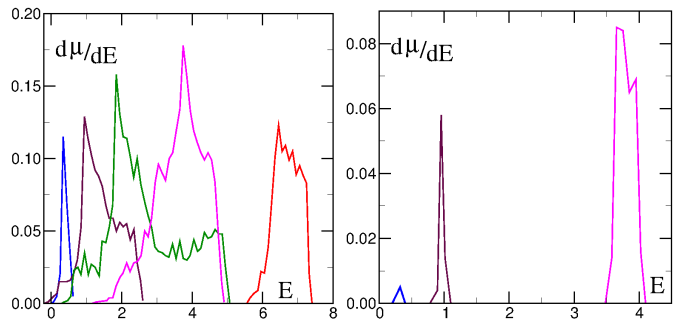


Fig. 6. Dependence of differential measure of diffusive trajectories $d\mu/dE$ on TIP energy E for: $\lambda = 2.5$ and $U = 1$ (blue), 3 (brown), 6 (green), 12 (magenta), 20 (red) with curves from left to right with corresponding total measure $\mu = 0.0252, 0.1319, 0.2295, 0.2420, 0.1190$ (left panel); $\lambda = 4.5$ and $U = 1$ (blue), 3 (brown), 12 (magenta) with corresponding total measure $\mu = 0.0005, 0.0076, 0.0333$ (right panel). Data are obtained from $N = 10^4$ trajectories homogeneously distributed in the phase space and iterated till time $t = 10^6$; averaging is done over energy interval $\Delta E = 0.1$.

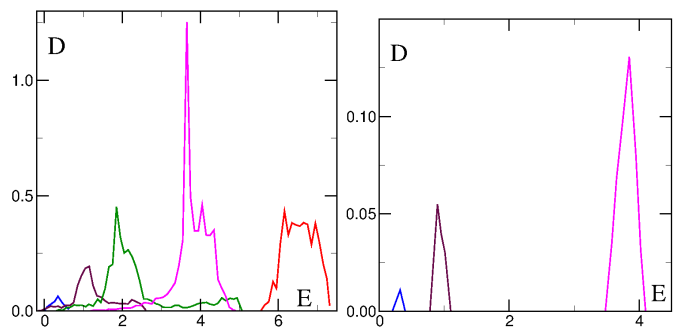


Fig. 7. Dependence of diffusion rate D on TIP energy E for same trajectories as in Fig. 6 at same parameters and colors with $\lambda = 2.5$ (left panel), $\lambda = 4.5$ (right panel).

at the same energies as in Figure 6, corresponding to developed chaos leading to TIP transitions between nearby cells. Since only a fraction of trajectories are delocalized the fluctuations of D from one trajectory to another are significant but averaging over trajectories inside histogram interval gives a reduction of such fluctuations. The diffusion rate can be also estimated as $D \approx (2\pi)^2/t_c$ where t_c is an average transition time between two cells. With typical value $D \sim 0.25$ we obtain $t_c/2\pi \sim 25$ being significantly larger than the period of small oscillations of one particle in a vicinity of potential minimum in (2). This shows that many TIP collisions are required to allow a jump from one cell to another.

For $\lambda = 4.5$ the results of Figures 6, 7 show that the measure of diffusive trajectories μ and their diffusion coefficient D are strongly reduced. Indeed, in this case the sum of kinetic terms of two particles is smaller than the potential barrier of one particle and thus the transitions of TIP from one cell to another can take place only in narrow regions of phase space (see Figure 3). This leads to small values of μ and D .

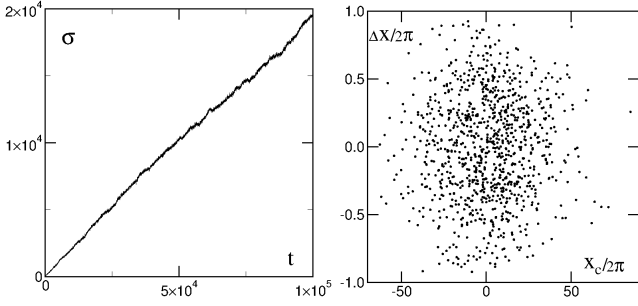


Fig. 8. Left panel: time dependence of the second moment $\sigma(t) = \langle ((x_1)^2 + (x_2)^2)/2 \rangle$ for the short range interaction model (6); data are averaged over 10^3 orbits taken in a chaotic component in a vicinity of energy $E = 3.32$ at $\lambda = 2.5$, $U = 6$, the fit gives the diffusion growth $\sigma = Dt + const$ with $D = 0.189 \pm 6 \times 10^{-5}$. Right panel: the distribution of $\Delta x = (x_2 - x_1)$ and $x_c = (x_1 + x_2)/2$ is shown for orbits of left panel at $t = 10^5$.

In view of a strong growth of p_1, p_2 and their large separation growing with time (see Figure 3 bottom panels) it is clear that, for the original Harper system of charged particles in 2D potential ($2\cos y + \lambda \cos x$) and a perpendicular magnetic field, there is no formation of diffusive TIP pairs due to separation of particles in y direction which is analogous to p in (3).

3 TIP with short range interactions in 1D

The one particle Hamiltonian (3) is strongly nonlinear and it is clear that practically any kind of interaction $U_2(x_1, x_2)$ between particles should lead to appearance of chaotic propulsion of TIP in coordinate space at $\lambda > 2$ when all one-particle orbits are bounded to one cell.

As an example we consider the short range interaction

$$U_2(x_1, x_2) = U \cos^2(\pi(x_2 - x_1)/2b), \quad |x_2 - x_1| \leq b; \\ U_2 = 0, \quad |x_2 - x_1| > b. \quad (6)$$

As in the previous section we use $b = 1$.

For this model an example of diffusive growth of the second moment σ is shown in Figure 8 for $\lambda = 2.5$, $U = 6$ and $E = 3.32$. For these values of λ and U the measure of delocalized orbits is found to be approximately $\mu \approx 0.1$ with $D \approx 0.15$ in the energy range $1 < E < 5$ and close to zero outside. At these parameters the separation between particles does not exceed the cell size (see Figure 8, right panel).

These results demonstrate that the chaotic delocalization of TIP in the 1D Harper model appears also in the case of short range interactions.

4 TIP with Coulomb interactions in 2D

Let us now consider the dynamics of TIP in the 2D classical Harper model. Without interactions the Hamiltonian is the sum of the Hamiltonian (3) in x and y directions.

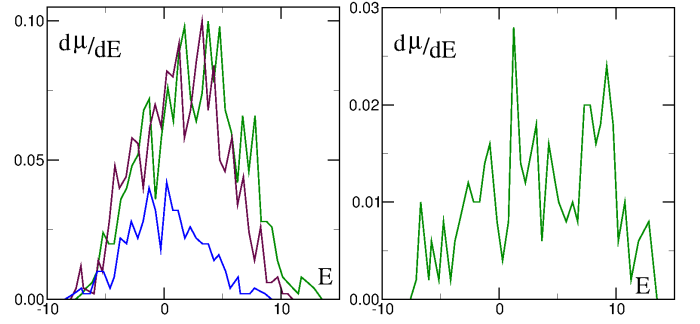


Fig. 9. Dependence of differential measure of diffusive trajectories $d\mu/dE$ on TIP energy E in the 2D Harper model for: $\lambda = 2.5$ and $U = 1$ (blue), 3 (brown), 6 (green) with corresponding total measure $\mu = 0.265, 0.796, 0.893$ (left panel); $\lambda = 4.5$ and $U = 6$ (green) with corresponding total measure $\mu = 0.217$, for $U = 3; 1$ the measure is small being respectively $\mu = 0.023; 0$ and these data are not shown (right panel). Data are obtained from $N = 10^3$ trajectories homogeneously distributed in the phase space and iterated till time $t = 4 \times 10^5$; averaging is done over energy interval $\Delta E = 0.5$.

As in 1D the dynamics of each particle is bounded to a one periodic cell. In presence of smoothed Coulomb interaction the TIP Hamiltonian has the form:

$$H(p_{x_1}, p_{x_2}, p_{y_1}, p_{y_2}, x_1, x_2, y_1, y_2) = \\ 2(\cos p_{x_1} + \cos p_{x_2} + \cos p_{y_1} + \cos p_{y_2}) \\ + \lambda(\cos x_1 + \cos x_2 + \cos y_1 + \cos y_2) \\ + U/((x_2 - x_1)^2 + (y_2 - y_1)^2 + b^2)^{1/2}. \quad (7)$$

As for 1D case we taken $b = 1$ in the following and $U \geq 0$. The available energy band is restricted to the interval $-8 - 4\lambda \leq E \leq 8 + 4\lambda + U$.

As for 1D the dynamics is integrated numerically with approximately the same accuracy. The measure of diffusive trajectories μ is obtained from 1000 orbits homogeneously distribution inside one cell followed till times $t = 4 \times 10^5$. The diffusive trajectories are defined as those that have a displacement larger than 3 cells during this time. The dependence of $d\mu/dE$ is shown in Figure 8 for $\lambda = 2.5; 4.5$ at $U = 1, 3, 6$. The total measure at $U = 6, \lambda = 2.5$ is increased comparing to the 1D case from $\mu = 0.23$ (1D, Figure 6) to $\mu = 0.89$ (2D, Figure 9). Indeed, due to a larger number of degrees of freedom in 2D the measure of chaos increases. However, for $\lambda = 4.5$ it becomes more difficult to penetrate through high potential barrier and there are practically no diffusive TIP at $U = 1, 3$.

The data of Figure 9 show the existence of an approximate mobility edge with diffusion inside the energy interval $E_{c_1} \approx -8 < E < E_{c_2} \approx 12$ (e.g. for $\lambda = 2.5, U = 6$). Of course, we should note that in 2D there are 4 degrees of freedom and the Arnold diffusion can still lead to a small measure of diffusive orbits along chaotic separatrix layers [35,36], but their measure drops exponentially for $E < E_{c_1}$ and $E > E_{c_2}$.

The dependence of the TIP diffusion coefficient D on energy E , determined from the relation $\sigma = Dt + const$,

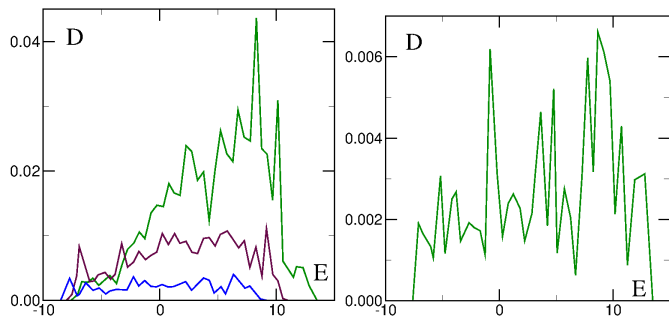


Fig. 10. Dependence of diffusion rate D on TIP energy E for same trajectories as in Fig. 9 at same parameters and colors with $\lambda = 2.5$ (left panel), $\lambda = 4.5$ (right panel).

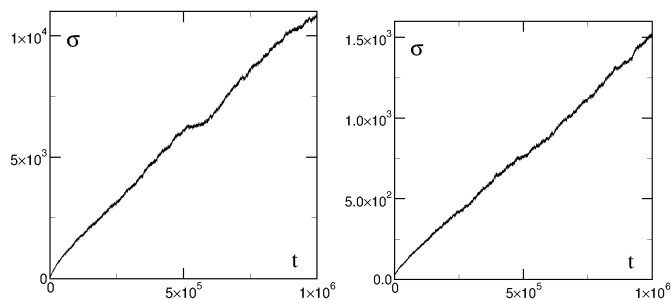


Fig. 11. Time dependence of the second moment $\sigma(t) = \langle ((x_1)^2 + (x_2)^2)/2 \rangle$ averaged over 500 orbits taken in a close vicinity to each other at $\lambda = 2.5$, $U = 6$, $E \approx -0.856$ (left panel) and $\lambda = 4.5$, $U = 12$, $E \approx 0.129$ (right panel). The fit gives the diffusion rate $\sigma = Dt + const$ with $D = 0.0106 \pm 3.7 \times 10^{-6}$ (left panel) and $D = 0.00143 \pm 3.8 \times 10^{-7}$ (right panel).

is shown in Figure 10 for parameters of Figure 9. The typical values of D in 2D are by factor 10 smaller than those in 1D (see Figure 7, e.g. at $\lambda = 2.5$, $U = 6$). We attribute this to a larger volume of chaotic motion so that an effective pressure of one particle on another, which allows to overcome the potential barrier, becomes smaller and TIP needs more time to find a narrow channel leading to a transition from one cell to another. For $\lambda = 4.5$ the diffusion D drops approximate in 10 times comparing to $\lambda = 2.5$ in the agreement with the fact that here very specific combinations of all coordinates are required to overcome the potential barrier.

Due to a small values of the diffusion rate D the fluctuations of μ and D are larger for 2D case comparing to 1D. An example of a more exact computation of D is shown in Figure 11 where the second moment σ is characterized by a linear growth with time reaching rather high values. Thus with large times and large number of trajectories the diffusion coefficient D is determined with a high precision. Even if σ in Figure 11 has large values corresponding to TIP displacement on a typical distance of 16 cells the maximal distance between two particles remains small $|\Delta x|/2\pi, |\Delta y|/2\pi < 2.5$ for $\lambda = 2.5$ and respectively 1.5 for $\lambda = 4.5$ at $t = 4 \times 10^5$.

An example of complex chaotic motion of TIP on small scales at $t \leq 10^4$ and $\lambda = 2.5$, $U = 6$ is shown in Figure 12.

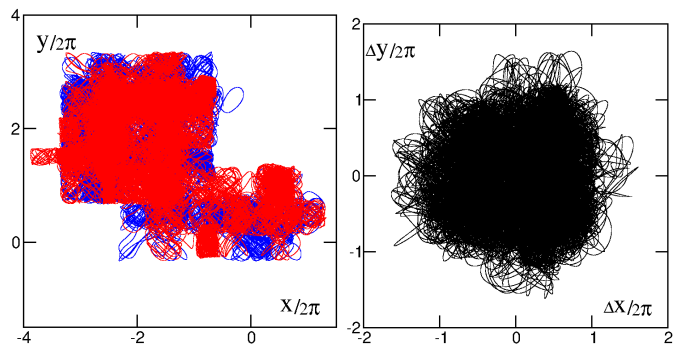


Fig. 12. Example of dynamics of one trajectory from Fig. 11 (left panel at $\lambda = 2.5$, $U = 6$, $E = -0.856$) for time $t \leq 10^4$ is shown on (x, y) plane with first particle in blue and second particle in red colors (left panel); the evolution of distance between particles $\Delta x = x_2 - x_1$, $\Delta y = y_2 - y_1$ is shown on right panel.

During this time particles make a displacement of up to 5 cells while the distance between them remains less than 2 cells.

The spreading of 10^3 TIP trajectories with time is illustrated in Figure 13. While with time TIP cover larger and larger area in (x, y) plane their relative distance in number of cells remains less than 2.5. Isolated fragments visible in the bottom left panel of Figure 13 are generated by trajectories which gained a large TIP displacement but then due to fluctuations are stacked in a few cells on the time interval of averaging $\delta t = 10^3$.

A more detailed verification of the validity of the Fokker-Planck equation in 2D (similar to Figure 5) requires averaging over larger number of trajectories and larger times due to smaller values of the diffusion coefficient D in 2D and we do not perform such a comparison here considering that the linear growth of the second moment on large times in Figure 11 provides a sufficient confirmation of the diffusive TIP propagation in the 2D Harper model.

Finally, we note that the chaotic dynamics is also found in numerical simulations with the kinetic TIP spectrum $p_1^2/2 + p_2^2/2$, instead of $2 \cos p_1 + 2 \cos p_2$ in (4) or (8). However, for such a spectrum at energies above the potential barrier it is found that particles become separated from each other with one escaping to infinity and another one remaining trapped by a potential so that a joint propagation of TIP is not detected in the cases which have been studied numerically.

5 Discussion

The presented results clearly show that for the classical Harper model in 1D and 2D the interactions between two particles lead to emergence of chaos and chaotic propulsion of TIP with their diffusive spreading over the whole lattice. Such an interaction induced diffusion appears in the regime when without interactions particle motion is bounded to one cell of periodic potential. For diffusive delocalized TIP dynamics the relative distance between par-

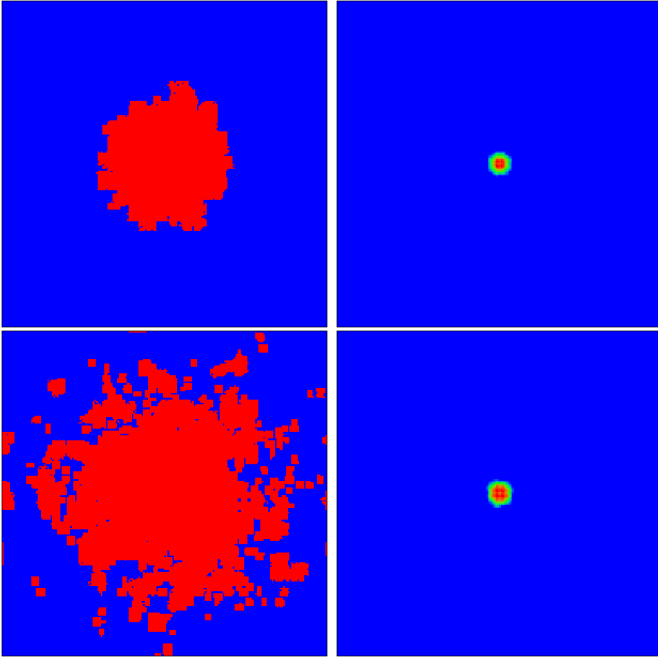


Fig. 13. Density distribution of TIP at parameters $\lambda = 2.5, U = 6, E = -0.856$ averaged over 10^3 trajectories. Left column: density of charge (sum over each particle) in the plane $(x/2\pi, y/2\pi)$ at time $t = 10^4$ at top panel and $t = 10^5$ at bottom panel (average over time interval $\delta t = 10^3$); right column: density distribution over distance between particles $\Delta x/2\pi = (x_2 - x_1)/2\pi, \Delta y/2\pi = (y_2 - y_1)/2\pi$ at time $t = 10^4$ at top panel and $t = 10^5$ at bottom panel (average over all times from zero to t). The panels show the squares $-16 \leq x/2\pi, y/2\pi \leq 16$ (left), $-16 \leq \Delta x/2\pi, \Delta y/2\pi \leq 16$ (right); at $t = 0$ TIP are located in one cell; color changes from blue (zero) to red (maximum).

ticles remains always smaller than the size of one to three periodic cells. In this sense the delocalized chaotic TIP represent a well defined new type of quasiparticles which we call *chaons* due to the chaos origin of their diffusive propagation over the whole system.

The chaon diffusion takes place inside a certain energy range of delocalized chaotic dynamics $E_{c_1} < E < E_{c_2}$ for a moderate interaction strength being comparable or even smaller than the one-particle energy band. Our results show that about a half of all energy band width can belong to delocalized dynamics. The energies E_{c_1}, E_{c_2} play a role of mobility edge in energy. Of course, at very weak interactions the KAM integrability is restored keeping the TIP dynamics bounded inside one periodic cell. Since the Harper model is strongly nonlinear the chaotic delocalization takes place for a broad range of interactions including the long range Coulomb interaction and a short range interaction.

The question about the quantum manifestations of this classical chaon delocalization is open for further investigations. It is possible that the quasiballistic FIKS pairs in the 1D quantum Harper model [24,25] appear as a result of quantization of classical chaons. Indeed, it is

known that in the quasiperiodic quantum systems, which are chaotic and diffusive in the classical limit, the quantization can create quasiballistic delocalized states like it is the case in the kicked Harper model (see results and Refs. in [37,38,39,40]). However, the investigations of quantum chaons and their possible relation with FIKS pairs requires further studies. The results presented in [24,25] are mainly done for the Hubbard interaction or a short range interaction on a discrete lattice and a semiclassical limit for such interactions is not so straightforward. Indeed, the semiclassical regime requires a smooth potential variation and a large number of quantum states n_q inside one potential period. It is possible that the semiclassical description can work even at moderate values of $n_q \sim 3$ but a detailed analysis of semiclassical description of such cases is required. The quantum interference effects may lead to the quantum localization of chaon diffusion in a similar way as for the Anderson localization of TIP in 1D and 2D (see discussions for TIP in disordered potential in [14,15,16,21]). However, in the case of quasiperiodic potential, appearing for irrational \hbar values, the situation is rather nontrivial as show the results of subdiffusive spreading for TIP in the 2D quantum Harper model [26].

The experimental investigations of diffusive chaons in the Harper model look to be promising. Indeed, the Aubry-André transition has been observed already with cold atoms in optical lattices and it has been shown that the interaction effects play here an important role [27,28,29]. The experimental progress with cold ions in optical lattices (see e.g. [41,42,43]) makes possible to study delocalized chaons with Coulomb interactions.

The author thanks Klaus Frahm for fruitful discussions of TIP properties and Vitaly Alperovich for discussions of possible realizations of considered Hamiltonian in semiconductor heterostructures.

References

1. P.G. Harper, Proc. Phys. Soc. London Sect. A **68**, 874 & 879 (1955).
2. M.Y. Azbel, Sov. Phys. JETP **19**, 634 (1964).
3. D.R. Hofstadter, Phys. Rev. B **14**, 2239 (1976).
4. S. Aubry and G. André, Ann. Israel Phys. Soc. **3**, 133 (1980).
5. J.B. Sokoloff, Phys. Rep. **126**, 189 (1985).
6. S.Y. Jitomirskaya, Ann. Math. **150**, 1159 (1999).
7. J. Bourgain, and S. Jitomirskaya, Invent. Math. **148**, 453 (2002).
8. A.Avila, S. Jitomirskaya and C.A.Marx, Ann. Math. arXiv:1602.05111v1[math-ph] (2016).
9. T. Geisel, R. Ketzmerick, and G. Petschel, Phys. Rev. Lett. **66**, 1651 (1991).
10. M. Wilkinson, and E.J. Austin, Phys. Rev. B **50**, 1420 (1994).
11. D.L. Shepelyansky, Phys. Rev. B **54**, 14896 (1996).
12. A. Barelli, J. Bellissard, Ph. Jacquod, and D.L. Shepelyansky, Phys. Rev. Lett. **77**, 4752 (1996).
13. G. Dufour, and G. Orso, Phys. Rev. Lett. **109**, 155306 (2012).
14. D.L. Shepelyansky, Phys. Rev. Lett. **73**, 2607 (1994).

15. Y. Imry, Europhys. Lett. **30**, 405 (1995).
16. D. Weinmann, A. Muller–Groeling, J.-L. Pichard, and K. Frahm, Phys. Rev. Lett. **75**, 1598 (1995).
17. K. Frahm, A. Muller–Groeling, J.-L. Pichard, and D. Weinmann, Europhys. Lett. **31**, 169 (1995).
18. F. von Oppen, T. Wetting, and J. Muller, Phys. Rev. Lett. **76**, 491 (1996).
19. F. Borgonovi, and D.L. Shepelyansky, J. de Physique I France **6**, 287 (1996).
20. K.M. Frahm, Eur. Phys. J. B, **10**, 371 (1999).
21. D.L. Shepelyansky, Phys. Rev. B **61**, 4588 (2000).
22. J. Lages, and D.L. Shepelyansky, Eur. Phys. J. B **21**, 129 (2001).
23. K.M. Frahm, Eur. Phys. J. B, **XX**, XXX (2016); arXiv:1602.08257[cond-mat.quant-gas] (2016).
24. S. Flach, M. Ivanchenko, and R. Khomeriki, Europhys. Lett. **98**, 66002 (2012).
25. K.M. Frahm, and D.L. Shepelyansky, Eur. Phys. J. B **88**, 337 (2015).
26. K.M. Frahm, and D.L. Shepelyansky, Eur. Phys. J. B **89**, 8 (2016).
27. G. Roati, C. D’Errico, L. Fallani, M. Fattori, C. Fort, M. Zaccanti, G. Modugno, M. Modugno, and M. Inguscio, Nature **453**, 895 (2008).
28. E. Lucioni, B. Deissler, L. Tanzi, G. Roati, M. Zaccanti, M. Modugno, M. Larcher, F. Dalfovo, M. Inguscio, and G. Modugno, Phys. Rev. Lett. **106**, 230403 (2011).
29. M. Schreiber, S.S. Hodgman, P. Bordia, H. Luschen, M.H. Fischer, R. Vosk, E. Altman, U. Schneider, and I. Bloch, Science **349**, 842 (2015).
30. P. Bordia, H.K. Luschen, S.S. Hodgman, M. Schreiber, I. Bloch, and U. Schneider, <http://arxiv.org/abs/1509.00478> (2015).
31. V.L. Pokrovsky and A.L. Talapov, *Theory of Incommensurate Crystals*, Harwood, London v.1 (1984).
32. G. Gruner, *Density Waves in Solids*, Addison-Wesley Publ. Company, New York (1994).
33. S.A.Brazovskii, *Ferroelectricity and charge ordering in quasi-1D organic conductors*, in *The Physics of Organic Superconductors and Conductors* A.Lebed (Ed.), p.313, Springer-Verlag, Berlin (2008).
34. V.L. Alperovich, N.T. Moshegov, V.A. Tkachenko, O.A. Tkachenko, A.I.Toropov, and A.S.Yaroshevich, Pis’ma ZhETF **70**, 112 (1999) [in Russian].
35. B.V. Chirikov, Phys. Reports **52**, 263 (1979).
36. A.J.Lichtenberg, M.A.Lieberman, *Regular and chaotic dynamics*, Springer, Berlin (1992).
37. R. Lima, and D.L. Shepelyansky, Phys. Rev. Lett. **67**, 1377 (1991).
38. R. Ketzmerick, K. Kruse, and T. Geisel, Physica D **131**, 247 (1999).
39. T. Prosen, I. I. Satija, and N. Shah, Phys. Rev. Lett. **87**, 066601 (2001).
40. R. Artuso, Scholarpedia **6(10)**, 10462 (2011).
41. P. Jurcevic, P. Hauke, C. Maier, C. Hempel, B.P. Lanyon, R. Blatt, and C.F. Roos, Phys. Rev. Lett. **115**, 100501 (2015).
42. A. Bylinskii, D. Gangloff, and V. Vuletic, Science **348**, 1115 (2015).
43. A. Bylinskii, D. Gangloff, I. Counts and V. Vuletic, Nature Materials doi:10.1038/nmat4601 (2016).